Novel Dynamical Magnetoelectric Effects in Multiferroic BiFeO 3

S. Omid Sayedaghaee, Bin Xu, Sergey Prosandeev, Charles Paillard, L. Bellaiche

Novel Dynamical Magnetoelectric Effects in Multiferroic $BiFeO_3$

S. Omid Sayedaghaee,[1,2] Bin Xu,[1,3] Sergey Prosandeev,[1,4] Charles Paillard,[1,5] and L. Bellaiche[1]

[1]*Physics Department and Institute for Nanoscience and Engineering, University of Arkansas, Fayetteville, Arkansas 72701, USA*

[2]*Microelectronics-Photonics Program, University of Arkansas, Fayetteville, Arkansas 72701, USA*

[3]*School of Physical Science and Technology, Soochow University, Suzhou, Jiangsu 215006, China*

[4]*Institute of Physics and Physics Department of Southern Federal University, Rostov-na-Donu 344090, Russia*

[5]*Laboratoire Structures, Proprits et Modlisation des Solides, CentraleSuplec, CNRS UMR 8580, Universit Paris-Saclay, 91190 Gif-sur-Yvette, France*

(Dated: February 18, 2019)

Abstract

An atomistic effective Hamiltonian scheme is employed within Molecular Dynamics simulations to investigate how the electrical polarization and magnetization of the multiferroic $BiFeO_3$ respond to time-dependent *ac* magnetic fields of various frequencies, as well as to reveal the frequency dependency of the dynamical (quadratic) magnetoelectric coefficient. We found the occurrence of vibrations having phonon frequencies in both the time-dependency of the electrical polarization and magnetization (for any applied *ac* frequency), therefore making such vibrations of electromagnonic nature, when the homogeneous strain of the system is frozen (case 1). Moreover, the quadratic magnetoelectric coupling constant is monotonous and almost dispersionless in the sub-THz range in this case 1. In contrast, when the homogeneous strain can fully relax (case 2), two additional low-frequency and strain-mediated oscillations emerge in the time-dependent behavior of the polarization and magnetization, which result in resonances in the quadratic magnetoelectric coefficient. Such additional oscillations consist of a mixing between acoustic phonons, optical phonons and magnons, and reflect the existence of a new quasiparticle that can be coined "electro-acoustic-magnon". This latter finding can prompt experimentalists to shape their samples to take advantage of, and tune, the magnetostrictive-induced mechanical resonance frequency, in order to achieve large dynamical magnetoelectric couplings.

Multiferroic materials can exhibit a magnetoelectric (ME) coupling between their electrical and magnetic moments. Such coupling is promising for designing novel devices by controlling magnetization with electric fields, or conversely, electrical polarization with magnetic fields [1–6]. Two paths can be taken to realize this magnetoelectric coupling: direct coupling of polarization with magnetic field vs mediated by strain. The latter is particularly investigated by mixing efficient magnetostrictive and piezoelectric materials, in composites [7] or heterostructures [8, 9].

These two types of coupling have been mostly for static properties [1–4, 10, 11]. In other words, how strain affects *dynamical* properties of multiferroics is mostly an uncharted territory. In particular, it is yet unclear whether ME coefficients can be improved with mechanical resonances in a single phase materials, as in laminar composites [8, 12]. It is also legitimate to investigate the effect of strain on electromagnons (mixing of phonons and magnons [13–16]), or even on the formation of novel type of (dynamical) objects.

To resolve such issues, we (1) conducted molecular dynamics (MD) simulations within an effective Hamiltonian scheme on $BiFeO_3$ (BFO), a prototypical multiferroic, subject to *ac* magnetic fields; and (2) monitored the resulting time-dependency of its electrical polarization and magnetization. It is found, that (i) electromagnons (of phonon frequencies) exist independently of allowing the homogeneous strain to relax; and (ii) relaxation of the homogeneous strain results in the emergence of a new type of quasiparticle consisting of acoustic vibrations coupled to phonons and magnons, and generating resonances in the quadratic ME coefficient.

Here, we use the effective Hamiltonian (H_{eff}) scheme of $BiFeO_3$ described in Ref. [17]. Its total energy $E_{\text{BFO}}(\{\boldsymbol{u}_i\}, \{\eta_H\}, \{\eta_I\}, \{\boldsymbol{\omega}_i\}, \{\boldsymbol{m}_i\})$ includes four types of degrees of freedom: 1) the local modes $\{\boldsymbol{u}_i\}$, proportional to the local electric dipoles [18, 19]; 2) the homogeneous $\{\eta_H\}$ and inhomogeneous $\{\eta_I\}$ strain tensors [18, 19]; 3) the pseudo-vectors $\{\boldsymbol{\omega}_i\}$ that characterize the oxygen octahedral tiltings [20] (also called antiferrodistortive (AFD) motions); and 4) the magnetic moments $\{\boldsymbol{m}_i\}$ of the Fe ions (in all cases, the subscript i labels unit cells in our simulated supercells). The total energy of H_{eff} for BFO is a sum of three main energies $E^{\text{tot}} = E^{\text{FE}}(\{\boldsymbol{u_i}\}, \{\eta_l\}) + E^{\text{AFD}}(\{\boldsymbol{u_i}\}, \{\eta_l\}, \{\boldsymbol{\omega_i}\}) + E^{\text{MAG}}(\{\boldsymbol{m_i}\}, \{\boldsymbol{u_i}\}, \{\eta_l\}, \{\boldsymbol{\omega_i}\})$, where $\{\eta_l\}$ is the total strain tensor (i.e., that incorporates both the homogenous and inhomogeneous components). E^{FE} is the energy involving the local modes and elastic deformations, while E^{AFD} is the energy that gathers the AFD motions and their couplings with local modes and

strains. Moreover, E^{MAG} contains the magnetic degrees of freedom and their couplings with local modes, AFD tiltings and strains, and reads [21]:

$$E^{\mathrm{MAG}} = \sum_{ij\alpha\gamma} Q_{ij\alpha\gamma} m_{i\alpha} m_{j\gamma} + \sum_{ij\alpha\gamma} S_{ij\alpha\gamma} m_{i\alpha} m_{j\gamma} + \sum_{ij,\alpha\gamma\nu\delta} E_{ij,\alpha\gamma\nu\delta} m_{i\alpha} m_{j\gamma} u_{i\nu} u_{i\delta} \quad (1)$$
$$+ \sum_{ij,\alpha\gamma\nu\delta} F_{ij,\alpha\gamma\nu\delta} m_{i\alpha} m_{j\gamma} \omega_{i\nu} \omega_{i\delta} + \sum_{ijl,\alpha\gamma} G_{ijl,\alpha\gamma} \eta_l(i) m_{i\alpha} m_{j\gamma} + \sum_{ij} L_{ij} (\boldsymbol{\omega}_i - \boldsymbol{\omega}_j) \cdot (\boldsymbol{m}_i \times \boldsymbol{m}_j) \ ,$$

where α, γ, ν, δ denote the Cartesian components, and the indices i and j run over sites. The six terms of Eq. (1) are, respectively, the dipolar interactions between the magnetic moments, the short-range magnetic exchange coupling, the coupling between the magnetic moments with local modes, AFD motions and strain, and a particular Dzyaloshinskii-Moriya (DM) interaction involving the oxygen octahedral tiltings. Under a magnetic field, an additional term $-\sum_i \boldsymbol{m}_i \cdot \boldsymbol{H}$ is also incorporated into the total energy. This effective Hamiltonian is then adopted for MD simulations, by solving the equations of motion for local modes, oxygen octahedral tilting, strains and magnetic moments, as detailed in Refs. [22–24]. We adopt a 12×12×12 supercell in terms of the 5-atom perovskite unit cell, with periodic boundary conditions. MD simulations are carried out at 1 K under the NPT ensemble when the homogeneous strain can relax during the simulations *versus* the NVT ensemble when the total strain is frozen during the computations. More details about the MD computations and the effective Hamiltonian schemes for BFO are given in the Supplemental Material [21, 25–36].

We apply to our considered state of BFO a magnetic field with two components, both aligned along the $[11\bar{2}]$ direction: a *dc* field of magnitude H_{dc}=245 T and an *ac* field given by $h_{ac}\sin(\omega t)$ where h_{ac}= 61.2 T and $\nu = \omega/2\pi$ is the frequency of the applied *ac* magnetic field. These fields are chosen to have high magnitude to numerically observe the response of polarization since ME coefficients are known to be rather small in $BiFeO_3$ [21, 32, 37, 38].

Let us first restrict ourselves to the case when the homogeneous strain is not allowed to relax (therefore adopting the homogeneous strain of the $R3c$ state under a sole *dc* magnetic field of 245 T) during the MD simulations – while the inhomogeneous strain can still vary. Figure 1a depicts the temporal behavior of the component of the polarization along the [111] direction in the *R3c* phase for a frequency (ν) of 160 GHz. Moreover, Fig. 1b displays the corresponding Fourier transform, and demonstrates that four main frequencies govern the temporal evolution of the electrical polarization: the applied *ac* frequency and its double

(i.e., 160 and 320 GHz), which reveals the occurrence of *dynamical* magnetoelectric effects, and two higher frequencies that are of the order of 4300 and 7000 GHz, which are natural *phonon* frequencies (see Refs. [22, 26, 39–46]).

Interestingly and as evidenced in Fig. 1d, these four frequencies also appear, in the Fourier transform of the curve representing the component of the magnetization along the $[11\bar{2}]$ direction as a function of time (shown in Fig. 1c). The frequency of 160 GHz seen in Fig. 1d emerges from the energy coupling the magnetic moment with the *ac* magnetic field, while the frequency at 320 GHz is characteristic of non-linear magnetic couplings. Remarkably, the high frequencies around 4300 GHz seen in Fig. 1d, and at lesser extent at 7000 GHz, reveal that natural phonons mix with magnons and affect the temporal evolution of the magnetization under a time-dependent magnetic field. Natural phonons thus become electromagnons [14–16], consistent with Ref. [47] for the $R\mathcal{3}c$ phase of $BiFeO_3$ – these electromagnons are presently numerically found to originate from the fact that polarization and oxygen octahedral tiltings affect the magnetic exchange parameters (third and fourth terms of Eq. (1)). Note that magnons having frequencies smaller than 160 GHz are not seen in Fig. 1d because the applied magnetic fields are too large and thus force the magnetic moments to mostly follow them, in addition to possessing smaller oscillations arising from the coupling of the magnetic moments with the aforementioned phonons (see Fig. 1c).

Let us now allow the homogeneous and inhomogeneous strains to fully relax during the MD simulations, and determine how it affects the temporal evolutions of the polarization and magnetization (see Figs 2a and 2c, respectively), as well as their Fourier transforms (*cf* Figs 2d and 2d, respectively). Figures 2e and 2f further report the variation of the diagonal elements of the homogenous strain tensor ($\eta_{H,1}$, $\eta_{H,2}$ and $\eta_{H,3}$) as a function of time and of their Fourier transforms, respectively, while Figs 2g and 2h provide similar information but for the shear elements of the homogeneous strain tensor ($\eta_{H,4}$, $\eta_{H,5}$ and $\eta_{H,6}$).

Remarkably, allowing the homogeneous strain to relax generates two *additional* frequencies in the Fourier transform of the polarization-*versus*-time curve with respect to the case of fixed homogeneous strains. These two frequencies are about 90 and 267 GHz, respectively, and can also be seen in the Fourier transform of the magnetization-*versus*-time functions. Figures 2h reveals that the frequency of 90 GHz originates from the oscillations of the shear elements of $\eta_{H,4}$, $\eta_{H,5}$ and $\eta_{H,6}$, while that of 267 GHz can be traced back to the vibrations of the diagonal ($\eta_{H,1}$, $\eta_{H,2}$ and $\eta_{H,3}$) elements of the homogeneous strain according to

Fig. 2f. Figures 2f and 2h further indicate that the diagonal and shear elements of the homogeneous strain tensor adopt the frequency of the applied magnetic fields of 160 GHz too, and that $\eta_{H,1}$, $\eta_{H,2}$ and $\eta_{H,3}$ also possess another frequency of the order of 67 GHz that slightly appears in the Fourier transform of the magnetization as shown in Fig. 2d (note that, on the other hand, we did not find any frequency higher than 320 GHz in the Fourier transforms of all homogeneous strain components, including the phonon frequencies). Comparing the results between the cases of the fixed *versus* relaxed homogeneous strain therefore demonstrates that, in our simulations, the homogeneous strain tensor has its own natural frequencies of the order of 90 and 267 GHz that then couple with oscillations of both the polarization and magnetization (note that these two frequencies are indeed natural frequencies of the homogeneous strain because they are also numerically found (not shown here) in the Fourier transform of the homogeneous strain when only a *dc* magnetic field is applied or even when no magnetic field is imposed on BFO, with the homogeneous strain having the possibility to relax during all these additional simulations). In other words, one can create a new type of quasiparticle mixing acoustic phonons, optical phonons and magnons, when applying *ac* magnetic fields with specific frequencies (i.e., 90 and 267 GHz here). Such creation of this quasiparticle can be understood as follows: the magnetic field at these frequencies naturally activates magnons, via the direct interaction between magnetic field and magnetic moments, which in turn dynamically couple with the strain and its natural frequencies via the magnetostrictive effect. This dynamical strain then activates optical phonons at these frequencies, because of couplings between strain and electrical dipoles (via electrostrictive and piezoelectric effects), therefore resulting in the formation of this quasiparticle. We propose to name such quasiparticle as "electro-acoustic-magnons" to emphasize that, unlike "traditional" electromagnons, strain also plays a role in their creation. Note that pump-probe experiments revealed acoustic excitations having similar frequencies than our predicted "electro-acoustic-magnons", namely around 30 GHz and 50 GHz for transverse and longitudinal acoustic modes in BFO respectively [48, 49] (note also that the presently calculated natural frequencies of the "electro-acoustic-magnons" naturally depend on the choice of the homogeneous strain mass adopted in our MD simulations). Moreover, a peak at about 300 GHz has been observed in the Raman spectrum of the spin-canted magnetic structure of epitaxial BFO films [36]. Furthermore, a phenomenon analogous to our proposed "electro-acoustic-magnons" has just been reported in Ref. [50], that is a dynamical coupling

between nuclear spins and electromechanical phonons. Such phenomenon consists of applying an *ac* electric field at the natural frequency of a resonator, which leads to an electrically tunable phonon that imparts diagonal and shear strains oscillating with time and which then dynamically couple with spins of nuclei (via a quadruple interaction between strains and spins there). This resulting dynamical coupling between spins and electromechanical phonons was indicated to open up quantum state engineering, such as coherent coupling between sound and nuclei and mechanical cooling of solid-state nuclei [50]. Such interesting possibilities therefore hint that our presently discovered "electro-acoustic-magnons" may lead to novel and important devices.

Let us now reveal how these "electro-acoustic-magnons" affect the dynamical magnetoelectric coefficients. For that, let us first recall the following equation of any component i of the polarization under magnetic fields [51, 52]: $P_i = P_i^s + \alpha_{ij}H_j + \frac{1}{2}\beta_{ijk}H_jH_k$, in which P_i^s is the i component of the spontaneous polarization, while H_j and H_k are components of the magnetic field. Moreover, α_{ij} and β_{ijk} are linear and quadratic magnetoelectric coefficients, respectively. Assuming that the linear ME coefficient is negligible compared to the quadratic coefficient (as suggested in Refs. [21, 53] for large fields) leads to the following equation for the polarization (along the [111] direction) when applying a magnetic field (along the $[11\bar{2}]$ direction) $H = H_{dc} + h_{ac}e^{i(\omega t - \frac{\pi}{2})}$:

$$P(t) = P_0 + \beta(0,\omega)H_{dc}h_{ac}e^{i(\omega t-\frac{\pi}{2})} + \beta(\omega,\omega)\frac{1}{2}h_{ac}^2e^{i(2\omega t-\pi)} \quad (2)$$

The second and third terms on the right-hand side of Eq.(2) characterize the magnetic-field induction of a polarization component with the same frequency of applied *ac* magnetic field and a second harmonic generation, respectively – which explains the occurrence of a strong Fourier transform at 160 GHz and a weaker one at 320 GHz in Figs. 1b and 1d. Note that Fig. 1a also shows the fit of $P(t)$ by a function of the form $A + B\sin\omega t$ by means of a solid line. Such fit nicely goes throughout the numerical MD data, therefore implying that (i) the linear ME coefficient and $\beta(\omega,\omega)$ can be neglected in front of $\beta(0,\omega)$ for the *ac* frequency of 160 GHz (the deviation of the MD data with respect to the fit consists of rapid oscillations associated with the phonon frequencies of about 4300 and 7000 GHz); and (ii) the validity of Eq. (2) is confirmed by our MD data.

Taking now into account that $\beta(0,\omega)$ is a complex number (especially close to resonant frequencies) we rewrite $\beta(0,\omega) = \beta'(0,\omega) + i\beta''(0,\omega)$, whose separate contributions can be

computed thanks to Eq. (2) via:

$$\beta'(0,\omega) = \frac{\frac{2}{L}\int_0^L (P(t)-P_0)\sin\omega t dt}{H_{dc}h_{ac}} \quad and \quad \beta''(0,\omega) = \frac{\frac{2}{L}\int_0^L (P(t)-P_0)\cos\omega t dt}{H_{dc}h_{ac}} \qquad (3)$$

where L is the overall simulation time.

We now apply, in addition to the *dc* magnetic field of 245 T, *ac* magnetic fields of the same magnitude of 61.2 T than in Figs 1 and 2 but of different frequencies ranging between 20 GHz and 500 GHz (both fields applied along $[11\bar{2}]$). Using Eqs (3), $\beta(0,\omega)$ is determined in the frozen (Fig. 3a) and relaxed (Fig. 3b) homogeneous strain cases. When the homogeneous strain is fixed in the simulations, the imaginary part of $\beta(0,\omega)$ is basically null for any *ac* frequency while the real part $\beta'(0,\omega)$ is nearly independent of the frequency taking a value of about 2.0×10^{-8} C/m^{2}T^2 $= 0.32\times10^{-19}$ s/A in magnitude – that agrees very well with the β_{311} coefficient of 0.3×10^{-19} s/A measured in Ref. [38]. On the other hand, when the homogeneous strain fully relaxes, $\beta(0,\omega)$ exhibits two resonances at precisely the two frequencies of the electro-acoustic-magnons, as evidenced by strong peaks of the $\beta''(0,\omega)$ imaginary part at 90 and 267 GHz that are accompanied by strong negative values immediately followed by strong positive values of the $\beta(0,\omega)'$ real part in the near vicinity of these two frequencies. Relaxing the homogeneous strain has thus dramatic consequences on the dynamical quadratic ME coefficients near some resonant frequencies because such strain dynamically couples with both the polarization and magnetization. The divergences of $\beta(0,\omega)$ at these two resonances that are induced by indirect (i.e strain-mediated) ME coupling therefore differ in nature from the divergences of the linear dynamical ME coefficient predicted to occur at magnons or phonon frequencies in Ref. [54] since these latter originate from a *direct* coupling between polarization and magnetism. Note that electromechanically mediated resonance in magnetoelectric coefficients was already observed in laminar piezoelectric-magnetoelectric composite structures [8, 12]. Here, it is of interest in the design of magneto-electric based sensors, for which the resonance frequency can be tuned by properly designing the shape and size of a *single phase* material (such as $BiFeO_3$).

Note also that we are unable to extract $\beta(0,\omega)$ for high frequencies, because the time dependency of the polarization becomes noisy due to interference between the phonon frequencies and the applied magnetic field frequency. This explains why we limited ourselves to frequencies up to 500 GHz in Fig. 3 and prevents us from checking if $\beta(0,\omega)$ has also resonances at the phonon/electromagnons frequencies of about 4300 and 7000 GHz.

In summary, molecular dynamics effective Hamiltonian simulations predicting the response of the polarization and magnetization to time-dependent magnetic fields of different *ac* frequency, allowed to extract the dispersion of the quadratic ME coefficient up to 500 GHz. In particular, electromagnons having phonon frequencies are found whether the homogeneous strain is frozen or relaxed during the simulations. Strain-mediated resonances in the magnetoelectric coupling are also reported, and are of large interest to design devices with proper shape of the sample for dynamical applications, since such shape can tune the resonant mechanical frequencies [55]. Those resonances can be described by a new type of quasiparticle that we coin "electric-acoustic-magnon", which arises when the frequency of the *ac* magnetic field resonantly excites homogeneous strain modes. This quasiparticle consists of a mixing of acoustic phonon, optical phonon and magnon. The calculations reported in this manuscript were done at very low temperature and high magnitude of the magnetic fields in order to have less fluctuation of the order parameters (e.g., polarization and magnetization) – yielding less numerical noise and thus better accuracy for the magnetoelectric response. However, as shown in the Supplementary Materials, our findings (e.g., resonances in the quadratic magnetoelectric coefficients originating from our discovered "electro-acoustic-magnons") still qualitatively hold at 300K and also for smaller magnetic fields. We strongly believe that these results are not only relevant to $BiFeO_3$ but rather to many multiferroics due to couplings between polarization, magnetization and strains in such systems. We thus hope that the present results deepen the current knowledge of multiferroics, in general, and of dynamical magneto-electric effects, in particular.

S.O.S. and L.B. thank the DARPA Grant No. HR0011- 15-2-0038 (under the MATRIX program). B.X. acknowledges funding from Air Force Office of Scientific Research under Grant No. FA9550-16-1-0065. S.P. thanks ONR Grant No. N00014-17-1-2818. C.P. acknowledges the ARO grant W911NF-16-1-0227. Some computations were also made possible owing to MRI Grant No. 0722625 from NSF, ONR Grant No.N00014-15-1-2881 (DURIP), and a Challenge grant from the Department of Defense. S.P. also appreciates support of RMES 3.1649.2017/4.6 and RFBR 18-52-00029_Bel_a.

[1] T. Zhao, A. Scholl, F. Zavaliche, K. Lee, M. Barry, A. Doran, M. P. Cruz, Y. H. Chu, C. Ederer, N. A. Spaldin, R. R. Das, D. M. Kim, S. H. Baek, C. B. Eom, and R. Ramesh, Nat.

Mater. **5**, 823 (2006).

[2] D. Lebeugle, D. Colson, A. Forget, M. Viret, A. M. Bataille, and A. Gukasov, Phys. Rev. Lett. **100**, 227602 (2008).

[3] W. Eerenstein, N. D. Mathur, and J. F. Scott Nature **442**, 759 (2006).

[4] M. Fiebig, T. Lottermoser, D. Frhlich, A. V. Goltsev, and R. V. Pisarev, Nature **419**, 818 (2002).

[5] N. Hur, S. Park, P. A. Sharma, J. S. Ahn, S. Guha, and S. W. Cheong, Nature **429**, 392 (2004).

[6] T. Lottermoser, T. Lonkai, U. Amann, D. Hohlwein, J. Ihringer, and M. Fiebig, Nature **430**, 541 (2004).

[7] N. Ortega, A. Kumar, J. F. Scott, and R. S. Katiyar, Journal of Physics: Condensed Matter **27**, 504002 (2015).

[8] C. Popov, H. Chang, P. M. Record, E. Abraham, R. W. Whatmore, and Z. Huang, J. Electroceramics **20**, 53 (2008).

[9] P.-E. Janolin, N. A. Pertsev, D. Sichuga, and L. Bellaiche, Phys. Rev. B **85**, 140401 (R) (2012).

[10] J.-M. Hu, L.-Q. Chen, and C.-W. Nan, Advanced Materials **28**, 15 (2016).

[11] V. Garcia, M. Bibes, and A. Barthélémy, C. R. Phys. **16**, 168 (2015).

[12] U. Laletsin, N. Padubnaya, G. Srinivasan, and C. P. DeVreugd, Appl. Phys. A **78**, 33 (2004).

[13] G. Smolenskii and I. Chupis, Sov. Phys. Usp. **25**, 475 (1982).

[14] M. Cazayous, Y. Gallais, A. Sacuto, R. de Sousa, D. Lebeugle, and D. Colson, Phys. Rev. Lett. **101**, 037601 (2008).

[15] A. B. Sushkov, M. Mostovoy, R. Valdes Aguilar, S.-W. Cheong, and H. D. Drew, J. Phys. Condens. Matter **20**, 434210 (2008).

[16] R. Valdés Aguilar, M. Mostovoy, A. B. Sushkov, C. L. Zhang, Y. J. Choi, S.-W. Cheong, and H. D. Drew, Phys. Rev. Lett. **102**, 047203 (2009).

[17] S. Prosandeev, D. Wang, W. Ren, J. Íñiguez, and L. Bellaiche, Advanced Functional Materials **23**, 234 (2013).

[18] W. Zhong, D. Vanderbilt, and K. M. Rabe, Phys. Rev. Lett. **73**, 1861 (1994).

[19] W. Zhong, D. Vanderbilt, and K. M. Rabe, Phys. Rev. B **52**, 6301 (1995).

[20] I. A. Kornev, L. Bellaiche, P. E. Janolin, B. Dkhil, and E. Suard, Phys. Rev. Lett. **97**, 157601

(2006).

[21] D. Albrecht, S. Lisenkov, W. Ren, D. Rahmedov, I. A. Kornev, and L. Bellaiche, Phys. Rev. B **81**, 140401 (2010).

[22] D. Wang, J. Weerasinghe, and L. Bellaiche, Phys.Rev.Lett. **109**, 067203 (2012).

[23] S. Bhattacharjee, D. Rahmedov, D. Wang, J. Íñiguez, and L. Bellaiche, Phys. Rev. Lett. **112**, 147601 (2014).

[24] K. Patel, S. Prosandeev, and L. Bellaiche, npj Computational Materials **3**, 24 (2017).

[25] D. J. Evans, W. G. Hoover, B. H. Failor, B. Moran, and A. J. C. Ladd, Phys. Rev. A **28**, 1016 (1983).

[26] R. Haumont, J. Kreisel, P. Bouvier, and F. Hippert, Phys. Rev. B **73**, 132101 (2006).

[27] J. B. Neaton, C. Ederer, U. V. Waghmare, N. A. Spaldin, and K. M. Rabe, Phys. Rev. B **71**, 014113 (2005).

[28] I. C. Infante, S. Lisenkov, B. Dupé, M. Bibes, S. Fusil, E. Jacquet, G. Geneste, S. Petit, A. Courtial, J. Juraszek, L. Bellaiche, A. Barthélémy, and B. Dkhil, Phys. Rev. Lett. **105**, 057601 (2010).

[29] D. Rahmedov, D. Wang, J. Íñiguez, and L. Bellaiche, Phys. Rev. Lett. **109**, 037207 (2012).

[30] M. Ramazanoglu, W. Ratcliff, Y. J. Choi, S. Lee, S.-W. Cheong, and V. Kiryukhin, Phys. Rev. B **83**, 174434 (2011).

[31] M. Ramazanoglu, M. Laver, W. Ratcliff, S. M. Watson, W. C. Chen, A. Jackson, K. Kothapalli, S. Lee, S.-W. Cheong, and V. Kiryukhin, Phys. Rev. Lett. **107**, 207206 (2011).

[32] Y. F. Popov, A. K. Zvezdin, G. P. Vorbev, V. A. Murashev, and D. N. Racov, Jetp Lett **57**, 65 (1993).

[33] Y. F. Popov, A. Kadomtseva, G. Vorob'ev, and A. Zvezdin, Ferroelectrics **162**, 135 (1994).

[34] M. Tokunaga, M. Azuma, and Y. Shimakawa, J. Phys. Soc. Jpn. **79**, 064713 (2010).

[35] A. Agbelele, D. Sando, C. Toulouse, C. Paillard, R. John-son, R. Ruffer, A. Popkov, C. Carrétéro, P. Rovillain, J.-M. Le Breton *et al.*, Adv. Mater. **29**, 1602327 (2017).

[36] D. Sando, A. Agbelele, D. Rahmedov, J. Liu, P. Rovillain, C. Toulouse, I. C. Infante, A. P. Pyatakov, S. Fusil, E. Jacquet, C. Carrétéro, C. Deranlot, S. Lisenkov, D. Wang, J.-M. Le Breton, M. Cazayous, A. Sacuto, J. Juraszek, A. K. Zvezdin, L. Bellaiche, B. Dkhil, A. Barthélémy, and M. Bibes, Nat. Mat. **12**, 641 (2013).

[37] S. Lisenkov, I. A. Kornev, and L. Bellaiche, Phys. Rev. B **79**, 012101 (2009); **79**, 219902 (E)

(2009).

[38] C. Tabares-Munoz, J. P. Rivera, A. Bezinges, A. Monnier, and H. Schmid, Jpn. J. Appl. Phys. **24**, 1051 (1985).

[39] S. Kamba, D. Nuzhnyy, M. Savinov, J. Sebek, J. Petzelt, J. Prokleska, R. Haumont, and J. Kreisel, Phys. Rev. B **75**, 024403 (2007).

[40] H. Fukumura, S. Matsui, H. Harima, T. Takahashi, T. Itoh, K. Kisoda, M. Tamada, Y. Noguchi, and M. Miyayama, J. Phys.: Condens. Matter **19**, 365224 (2007).

[41] R. P. S. M. Lobo, R. L. Moreira, D. Lebeugle, and D. Colson, Phys. Rev. B **76**, 172105 (2007).

[42] D. Rout, K.-S. Moon, and S.-J. L. Kang, J. Raman Spectrosc. **40**, 618 (2009).

[43] J. Lu, M. Schmidt, P. Lunkenheimer, A. Pimenov, A. A. Mukhin, V. D. Travkin, and A. Loidl, J. Phys. Conf. Ser. **200**, 012106 (2010).

[44] R. Palai, H. Schmid, J. F. Scott, and R. S. Katiyar, Phys. Rev. B **81**, 064110 (2010).

[45] A. A. Porporati, K. Tsuji, M. Valant, A.-K. Axelsson, and G. Pezzotti, J. Raman Spectrosc. **41**, 84 (2010).

[46] J. Hlinka, J. Pokorny, S. Karimi, and I. M. Reaney, Phys. Rev. B **83**, 020101(R) (2011).

[47] C.-M. Chang, B. K. Mani, S. Lisenkov, and I. Ponomareva, Ferroelectrics **494**, 68 (2016).

[48] M. Lejman, G. Vaudel, I. C. Infante, I. Chaban, T. Pezeril, M. Edely, G. F. Nataf, J. Kreisel, V. E. Gusev, B. Dkhil, and P. Ruello, Nat. Comm. **5**, 4301 (2014).

[49] M. Lejman, G. Vaudel, I. C. Infante, P. Gemeiner, V. E. Gusev, B. Dkhil, and P. Ruello, Nat. Comm. **7**, 12345 (2016).

[50] Y. Okazaki, I. Mahboob, K. Onomitsu, S. Sasaki, S. Nakamura, N. Kaneko, and H. Yamaguchi, Nat. Comm. **9**, 2993 (2018).

[51] H. Schmid, International Journal of Magnetism **4**, 337 (1973).

[52] M. Fiebig, Journal of Physics D: Applied Physics **38**, R123 (2005).

[53] I. A. Kornev, S. Lisenkov, R. Haumont, B. Dkhil, and L. Bellaiche, Phys. Rev. Lett. **99**, 227602 (2007).

[54] K. L. Livesey and R. L. Stamps, Phys. Rev. B **81**, 094405 (2010).

[55] Note that the homogeneous strain tensor is a degree of freedom in our Molecular Dynamics simulations and is thus assigned a mass for its equation of motion. Consequently, it has its own natural frequencies in the infinite $BiFeO_3$ crystal, which is our presently studied system (this fact is numerically confirmed by varying this mass, which results in the shift

of the mechanical and thus "electro-acoustic-magnon" frequencies). What is interesting is that mechanical frequencies are known to be practically dependent on the sample size. As a result, alternating the sample size should allow to control the frequencies of our discovered "electro-acoustic-magnons".

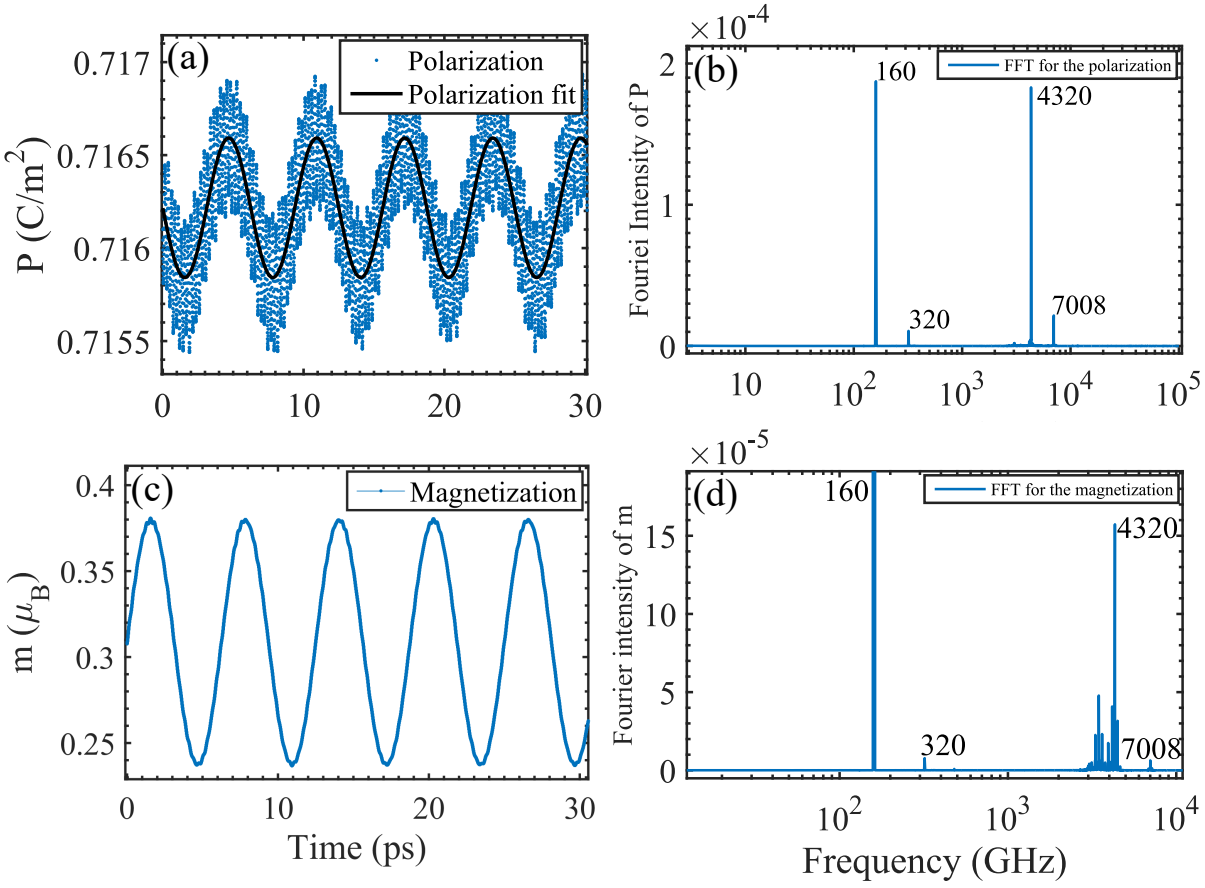

FIG. 1: (Color online) Temporal evolution of the polarization (panel a) and magnetization (panel c) in $BiFeO_3$ under a *dc* magnetic field of 245 T of magnitude coexisting with an *ac* magnetic field of 61.2 T of magnitude and of 160 GHz of frequency, along with their resulting Fourier transforms (panels b and d, respectively) as a function of frequency, in the case that the homogeneous strain is frozen in the MD simulations. The *dc* and *ac* magnetic fields are applied along the $[11\bar{2}]$ direction. The displayed polarization is along the [111] direction while the magnetization is along the $[11\bar{2}]$ direction. The solid line in Panel a represents the fit of the MD data by a function of the form $A + B\sin\omega t$ where $\omega/2\pi$=160 GHz.

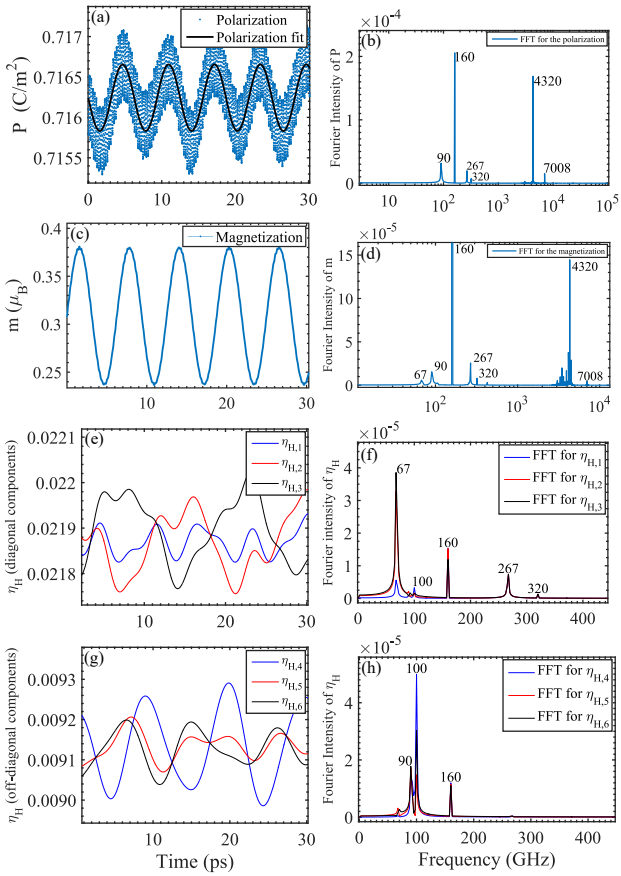

FIG. 2: (Color online) Temporal evolution of the polarization (panel a), magnetization (panel c), diagonal elements of the homogeneous strain tensor (panel e) and shear elements of the homogeneous strain tensor (panel g) in $BiFeO_3$ under a *dc* magnetic field of 245 T of magnitude coexisting with an *ac* magnetic field of 61.2 T of magnitude and of 160 GHz of frequency, along with their resulting Fourier transforms (Panels b, d, f and h, respectively) as a function of frequency, when the homogeneous strain is allowed to relax during the MD simulations. The *dc* and *ac* magnetic fields are applied along the $[11\bar{2}]$ direction. The displayed polarization is along the [111] direction while the magnetization is along the $[11\bar{2}]$ direction.

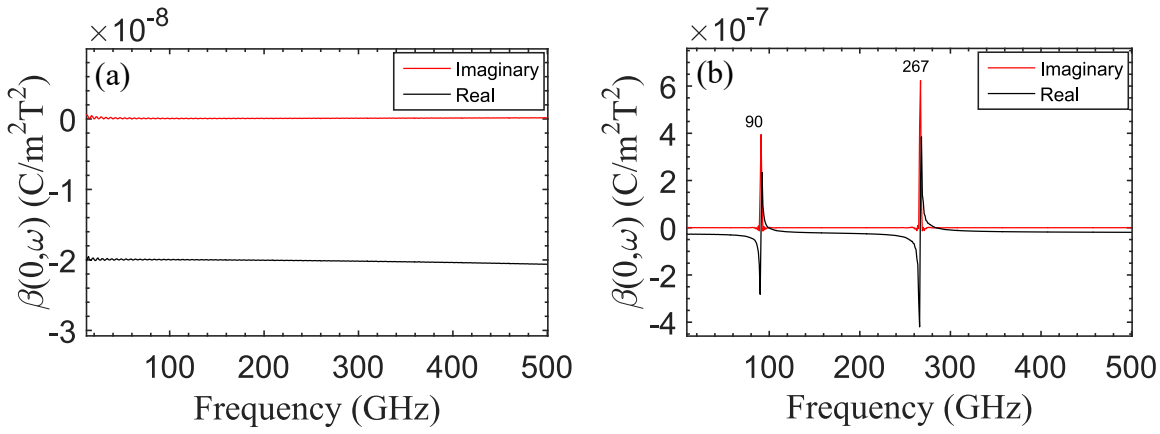

FIG. 3: (Color online) Dependency of the real and imaginary parts of the $\beta_{(0,\omega)}$ dynamical quadratic ME coefficient on the frequency of the *ac* applied magnetic field when the homogeneous strain is frozen (panel a) *versus* when the homogeneous strain can relax in the MD simulations (panel b).